

Article

Changes in the Optical Properties of an M-Doped (M = Pt, Ti) hBN Sheet and CO₂ Capturing

Juan Manuel Ramírez-de-Arellano ^{1,*} , Ali Fransuani Jiménez-González ²  and Luis Fernando Magaña ² ¹ Tecnológico de Monterrey, Escuela de Ingeniería y Ciencias, Calle del Puente 222, Mexico City 14380, Mexico² Instituto de Física, Universidad Nacional Autónoma de México, Mexico City 01000, Mexico

* Correspondence: jramirezdearellano@tec.mx

Abstract: We performed ab initio DFT calculations to explore the optical properties of a hexagonal boron nitride (hBN) monolayer, doped with a Ti or a Pt atom. Ti doping increases the adsorption capability of the boron nitride surface for capturing CO₂. Both doping types increase the optical absorption and reflectivity of the hBN surface in the infrared and visible regions. For the UV region, a B vacancy increases the absorption of the hBN sheet. Captured CO₂ bears substantial changes in the optical absorption and reflectivity spectra of the system considered.

Keywords: DFT; adsorption; CO₂; ab initio calculations; boron nitride; 2D materials



Citation: Ramírez-de-Arellano, J.M.; Jiménez-González, A.F.; Magaña, L.F. Changes in the Optical Properties of an M-Doped (M = Pt, Ti) hBN Sheet and CO₂ Capturing. *Crystals* **2022**, *12*, 1773. <https://doi.org/10.3390/cryst12121773>

Academic Editors: Fangfei Ming, Yaping Ma and Xuefeng Wu

Received: 15 November 2022

Accepted: 4 December 2022

Published: 7 December 2022

Publisher's Note: MDPI stays neutral with regard to jurisdictional claims in published maps and institutional affiliations.



Copyright: © 2022 by the authors. Licensee MDPI, Basel, Switzerland. This article is an open access article distributed under the terms and conditions of the Creative Commons Attribution (CC BY) license (<https://creativecommons.org/licenses/by/4.0/>).

1. Introduction

Hexagonal boron nitride (hBN) is a layered crystal; hBN bulk crystals show a significant distance (3.33 Å) between layers interacting via weak Van der Waals forces. Furthermore, epilayers of hBN are three-dimensional (3D) systems too. Notably, hBN crystals can be obtained by different methods, for example, by precipitation from a nickel-chromium flux with a boron nitride source [1].

There are several processes to obtain 2D hBN, such as gas phase epitaxy, exfoliation, chemical vapor deposition, and other methods. The distance of B-N is very similar to the C-C separation in graphene. Furthermore, it has considerable chemical inertness, mechanical robustness, thermal stability, and oxidation resistance. Furthermore, it has unique optoelectrical properties, with a wide band gap (around 6 eV). Thus, hBN looks promising—among other 2D materials—for the most advanced microelectronic technologies [2,3].

The role of 2D materials in removing pollutant molecules from the environment is a matter of current research as well because of their sizeable specific area for this purpose or to act as sensors.

In this study, we focus on the optical properties of a hexagonal boron nitride (hBN) nanosheet doped with a Pt or a Ti atom. The crystallographic structure of bulk hBN consists of alternating B and N atoms in hexagonal layers, with an AA stacking order. Conventional X-ray powder diffraction has been used to determine its lattice constants, which are $a = b = 2.50$ Å and $c = 6.661$ Å [4–7]. These values and its structure in general are quite similar to those of graphite.

However, the electronic structure and conduction properties are different. As is well known, hBN is a chemically stable material that has attracted great interest as an alternative for GaN in laser applications, as well as in new optoelectronic applications requiring high-quality 2D materials [8]. It has a direct band gap in the ultraviolet region. Studies have shown that a pristine hBN monolayer presents high reflectivity and insignificant absorption in the visible light spectrum. Additionally, an increased band gap increases the optical absorption for GaN, BN, and BGaN alloys, particularly in the ultraviolet region. The absorption of a hBN monolayer has also been theoretically described, showing that hBN could be adsorbed on quartz and graphite [9–11]. On the other hand, sheets of hBN

supported on metal substrates (e.g., Au, Cu, Pt) have been theoretically shown to enhance the hydrogen evolution reactions of the combined systems, such as for energy conversion and storage applications [12–15]. The optical properties of a Sn-doped hBN monolayer have also been explored via density functional theory (DFT)-based calculations, showing that the doping Sn atom helped increase the adsorption coefficient of the hBN surface [16].

In previous works, we found that both Pt and Ti can be adsorbed with ease at a vacancy of a hBN sheet, but only the Ti-decorated hBN sheet would be a good candidate for CO₂ capture [17]. In contrast to Sn doping, we used Pt and Ti doping because of the better catalytical properties and resistance to corrosion that these transition metals have [18]. Our main aim is to add useful knowledge to the development of pollutant sensors—in this case for CO₂—for environmental as well as optoelectronic applications. A more comprehensive review on the increased interest in hBN use in these fields can be found in the literature [8,15].

Other theoretical works have considered the stability of different metals—including Pt and Ti—supported on B-deficient hBN sheets, as well as their effects in hBN oxygen reduction reactions [19,20]. The relevance and novelty of our study, on the other hand, is to expand on this by considering both types of vacancies (removal of a B and an N atom). In our aforementioned previous work, we also included ab initio MD calculations as well as PDOS plots of the combined systems [17].

However, two questions remain that we investigate in this work: whether the optical properties of the hBN monolayer would change substantially by the Ti or Pt doping; and how the CO₂ adsorption modifies the optical properties of the system.

2. Materials and Methods

We used Quantum ESPRESSO, an open-source, free software package [21], to perform calculations based on DFT [22–24], within the pseudopotential formalism. The code suite used considers periodic boundary conditions and plane-wave expansions. Martin–Troulliers norm-conserving pseudopotentials [25] and the Perdew–Burke–Ernzerhof (PBE-GGA) exchange–correlation functional were considered [26].

The valence electronic states are considered in the same way as in previous studies of Pt- and Ti-doped hBN [17]: for oxygen: $2s^2 2p^4$; nitrogen: $2s^2 2p^3$; boron: $2s^2 2p^1$; platinum: $6s^1 5d^9$; titanium: $3s^2 3p^6 3d^2 4s^2$; and carbon: $2s^2 2p^2$. The energy cutoff was 80 Ry (≈ 1100 eV), and we took a k-point mesh of 40 k points within the Monkhorst–Pack scheme [27]. The threshold energy for the convergence of the SCF calculations was set to 1.0×10^{-6} eV.

As we were not interested in the magnetic properties of the system, we used non-relativistic, non-polarized spin calculations, which previous studies show does not affect the kind of properties considered in this work [28]. The unit cell consists of 50 atoms forming the hBN monolayer, with cell parameters being $a = b = 12.49$ Å, and to ensure a vacuum along the z-axis, $c = 26.39$ Å. As a reference, Figure 1 shows all the cases considered in this work. Figure 2 shows the unit cell and a summary of the calculations previously done on this system, the details of which can be found in [17], of which this work is a continuation.

The imaginary component dielectric tensor was calculated within the random phase approximation [29] and using the Kramers–Kronig relations [30]. We obtained, subsequently, the absorption and reflectivity for each case. We considered a propagation direction of the electromagnetic wave that was perpendicular to the hBN sheet. The details of the procedure used to calculate the optical spectra are in [31]. Finally, XCrySDen software was used for visualization purposes [32].

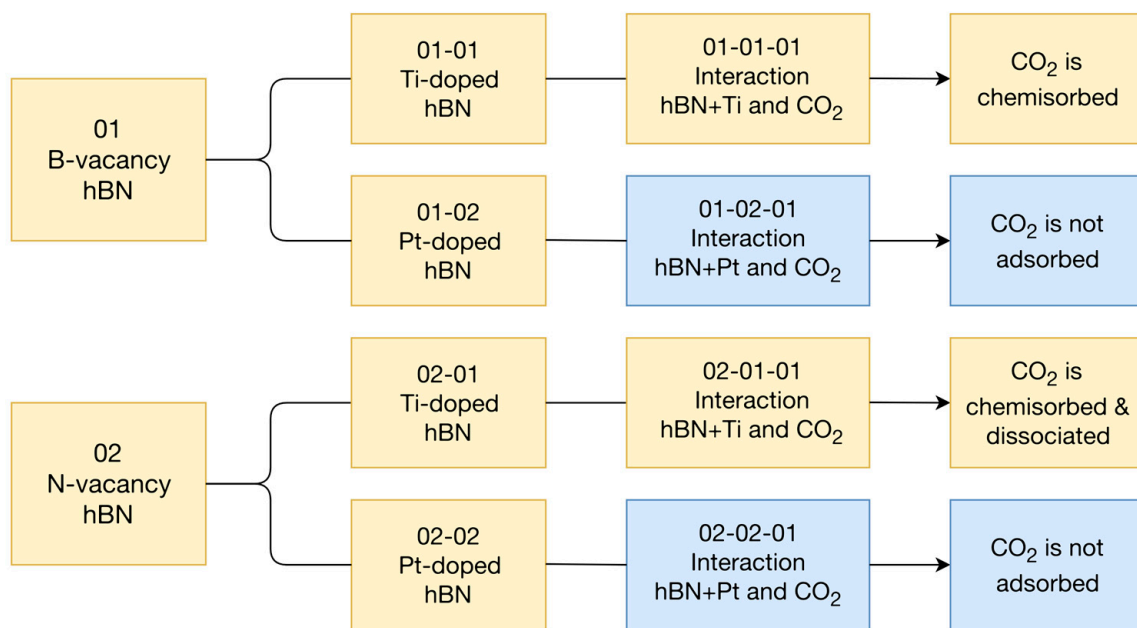
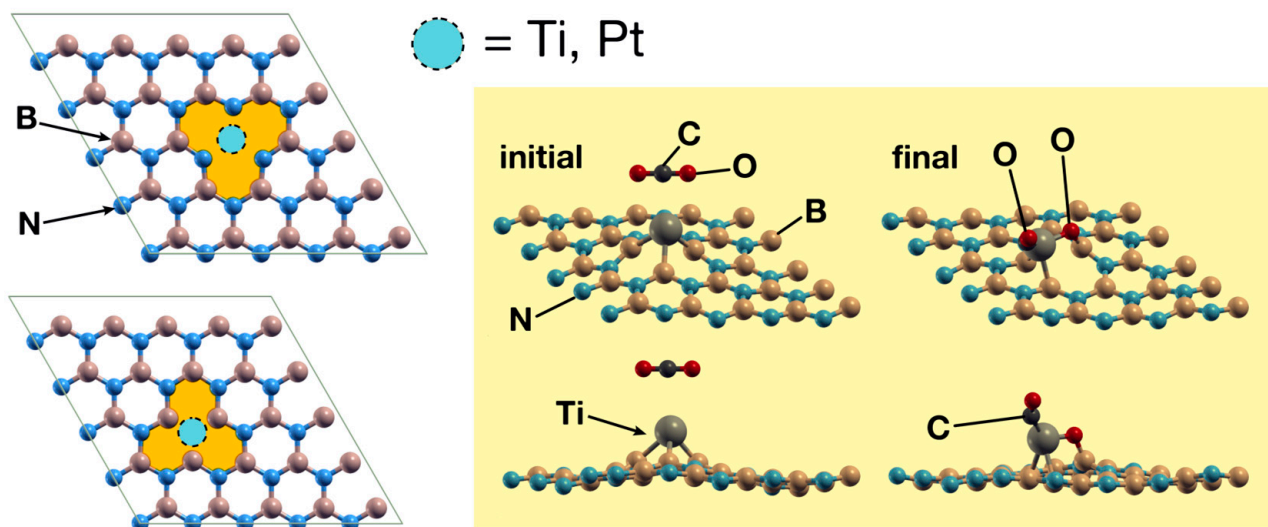


Figure 1. Diagram of the cases considered in this work. The interactions refer to FPMD calculations performed on [17]. This work builds from there to explore the optical properties of the resultant systems.

Ti or Pt absorbed in B and N vacancies of hBN surface



The Ti-doped case has a larger catalytic effect for CO₂ capture

Figure 2. The main results presented on the previous work [17] from which this work builds. Ti-doped hBN showed a larger ability to capture CO₂, compared to Pt doping.

3. Results

We calculated the optical absorption spectra in the infrared (see Figure 3), visible (see Figure 4), and ultraviolet range (see Figure 5) along the Z-axis. The spectra give the horizontal axis in eV units (equivalent to 8066.666 cm^{-1}).

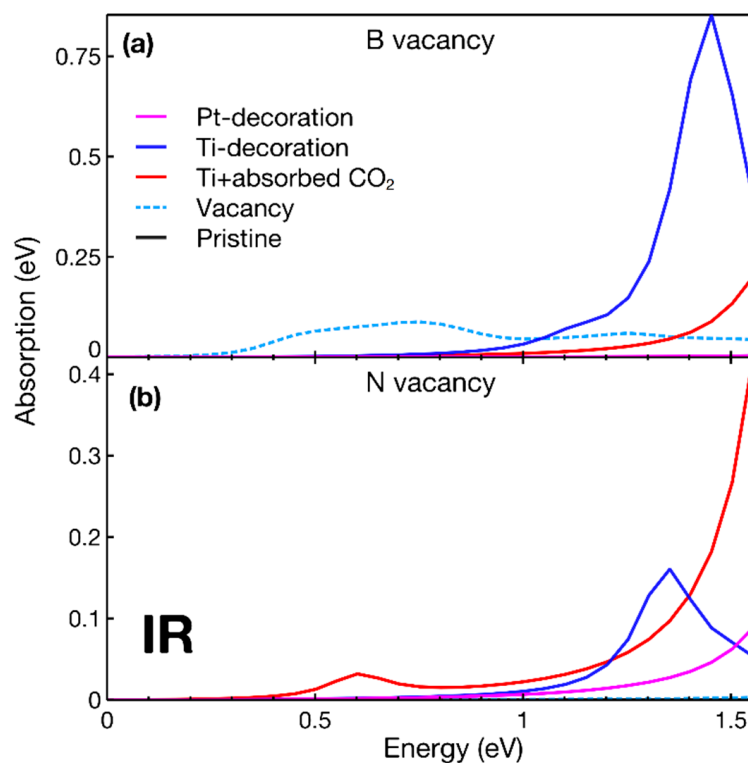


Figure 3. Absorption in the infrared region for the cases considered. In (a) we see the cases with the B atom removed from the hBN surface, while in (b) we see those with the N atom removed. There is an acute increase in the absorption when titanium is a dopant. There is also a high response for CO₂.

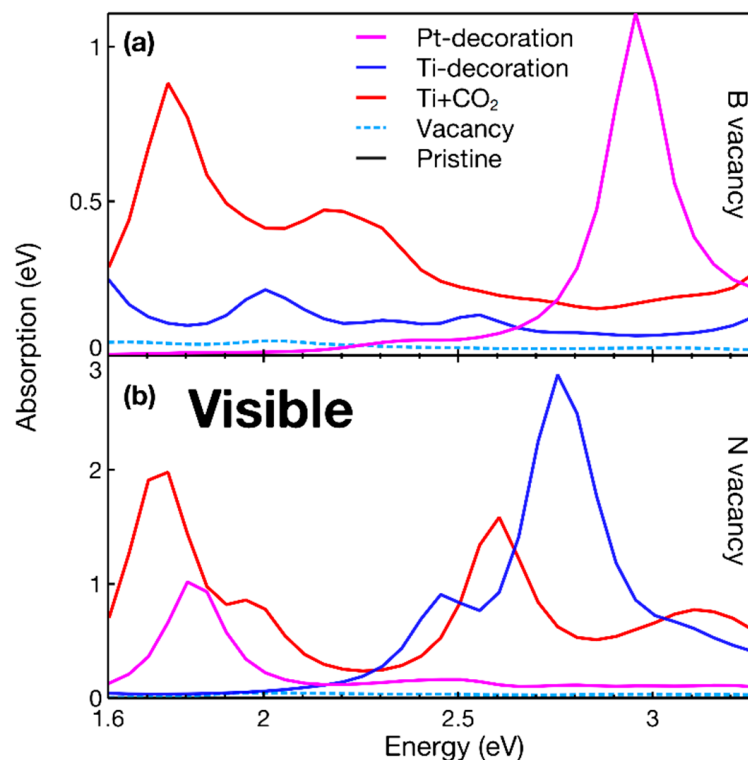


Figure 4. Absorption in the visible region for the cases considered. In (a) we see the cases with the B atom removed from the hBN surface, while in (b) we see those with the N atom removed. The Ti decoration in place of an N vacancy in the hBN surface significantly increases the optical absorption in this range. The Pt decoration has a similar, though less noticeable, effect.

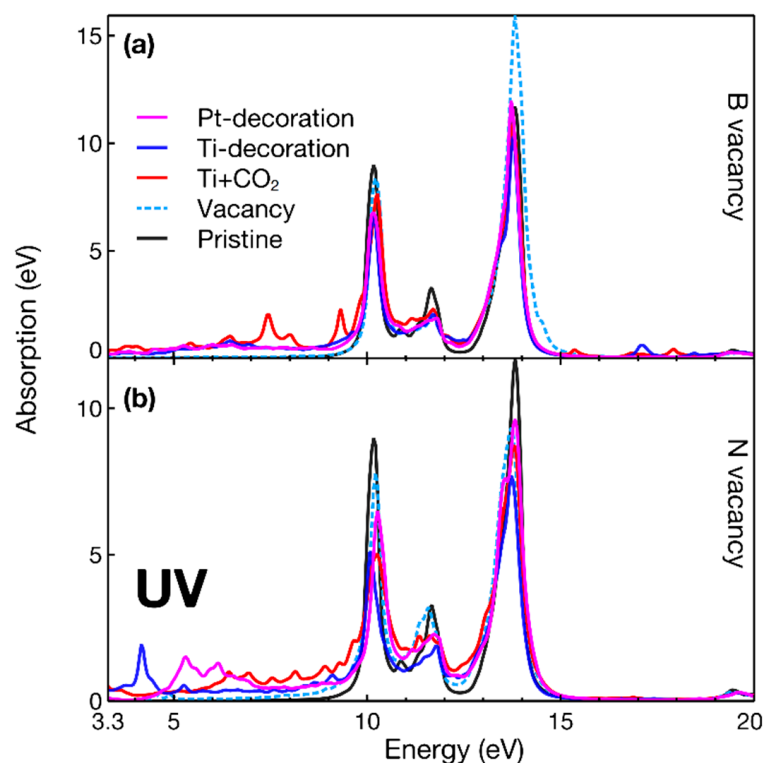


Figure 5. Absorption in the ultraviolet region for the cases considered. In (a) we see the cases with the B atom removed from the hBN surface, while in (b) we see those with the N atom removed. The introduction of a B vacancy increases the absorption, but otherwise the response appears unchanged across cases.

From Figure 3, the pristine hBN monolayer shows no absorption in the IR region. Creating a B vacancy in the hBN surface increases its absorption at the IR level by a small amount (less than 0.10 eV), while the N vacancy has a negligible effect on it. However, the substitutionally absorbed Ti atom causes a larger increase in the adsorption, reaching up to 0.85 eV at the near-IR region (1.50 eV) for the B vacancy case. The chemisorbed CO_2 reduces this peak by four.

For the N vacancy case—which shows no IR absorption—the effect of the Pt doping is relatively small, showing an absorption peak of around 0.08 eV in the near-IR region, but the Ti doping shows a larger increase, reaching a height of 0.16 eV. The chemisorbed and dissociated CO_2 molecule adds the most significant growth among the N vacancy cases, reaching a peak of 0.40 eV.

For the visible region (Figure 4), creating a B vacancy allows the hBN layer to absorb in all this range; but the effect of the Pt and Ti doping is particularly large. For the B vacancy hBN monolayer (Figure 4a), the Pt doping has a more significant effect than the Ti doping alone in terms of the absorption increase for this region. The Pt doping case shows an absorption peak of 1.10 eV for violet (corresponding to an energy of 3.00 eV), while the Ti doping results in two smaller maxima of around 0.21 eV for red (at an energy of 1.60 eV) and orange (2.00 eV) absorption. However, the hBN+Ti+ CO_2 system also shows a large increase in the absorption at this region, with a peak of 0.88 eV for red absorption (at an energy of 1.75 eV), and a smaller peak of 0.46 eV for green absorption (at 2.20 eV).

For the N vacancy (Figure 4b), the Ti-doping results in the most significant increase, showing an absorption peak of 2.75 eV corresponding to blue absorption (2.30 eV) and a second, smaller absorption peak of 0.90 eV at 2.75 eV (cyan). After that case, the second and third largest maxima are reached for the hBN+Ti+ CO_2 case (labeled “02-01-01” in Figure 1). These two peaks are at the absorption of 1.97 eV for red absorption (at an energy

of 1.75 eV) and 1.58 eV for blue (at 2.60 eV). The Pt doping results in a minor increase, with an absorption peak of 1 eV for red absorption (at an energy of 1.8 eV).

The UV region shows relatively small changes across the cases considered, although the B vacancy case (Figure 5) stands out, as the creation of the vacancy brings a significant absorption increase of +4.2 eV compared to the second largest. For both vacancies, the system hBN+Ti+CO₂ (labeled as “01-01-01” and “02-01-01” in Figure 1) increases absorption for the near, deep, and vacuum UV regions, corresponding to energies from 4.00 to 9.60 eV.

Finally, the pristine hBN reflectivity shows three peaks: the first at an energy of 10.2 eV, the second at 11.1 eV, and the third at 13.9 eV. Creating a B vacancy (Figure 6a) increases the third peak by around 50%, while the Pt doping and Ti-doping reduce the first peak by the same amount approximately. However, for both Pt and Ti-doping, additional peaks are observed. The chemisorbed CO₂ molecule (case “01-01-01” in Figure 1) results in a shift of the peaks introduced by the Ti doping but no relevant change in its absorption magnitude.

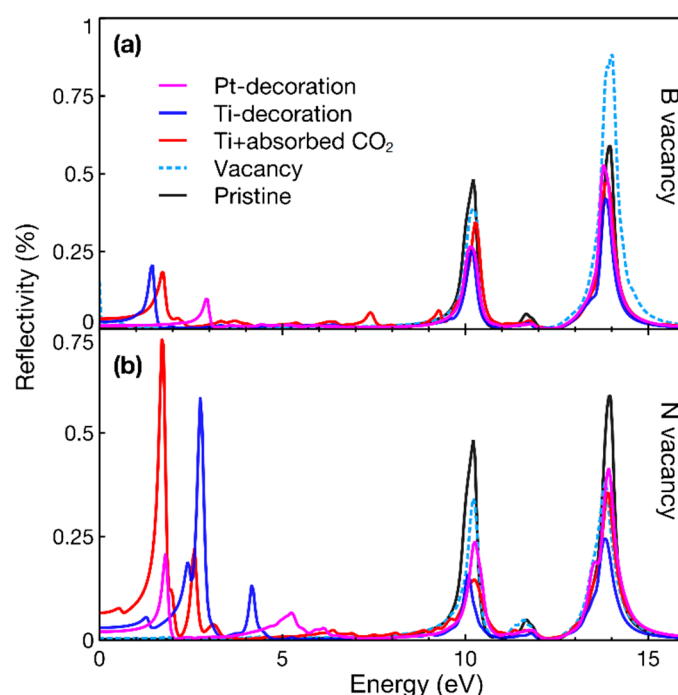


Figure 6. Reflectivity spectra. In (a) we see the cases with the B atom removed from the hBN surface, while in (b) we see those with the N atom removed. The effect of the Pt and Ti doping and the CO₂ interaction is particularly evident for the N vacancy hBN case.

The N vacancy (Figure 6b) results in a slight decrease in reflectivity, particularly in the first and third peaks of the pristine hBN. The Pt and Ti doping effect is similar to that for the B vacancy hBN, with a reduction of around 50% of the three original peaks, but new maxima appear in the energy region from 0.00 to 5.00 eV. These peaks are almost four times larger than those for the B vacancy hBN. The hBN+Ti+CO₂ system (case “02-01-01” in Figure 1) increases the reflectivity peak introduced by the Ti doping alone by around 25%, shifting it from an energy of 2.70 eV to 1.70 eV.

4. Discussion

We explored the optical properties of an hBN monolayer. There is a substantial change in the optical absorption of the hBN monolayer in the infrared and visible regions with Pt or Ti doping. The reflectivity increases in the same ranges, particularly for the N vacancy hBN with Ti doping and CO₂ absorption. The changes in the optical properties we found indicate that the systems explored could be good candidates for CO₂ sensing. At the same time, Pt or Ti doping could benefit optoelectronic applications.

Author Contributions: Conceptualization: L.F.M., A.F.J.-G., and J.M.R.-d.-A.; Data curation: A.F.J.-G. and J.M.R.-d.-A.; Formal analysis: L.F.M., J.M.R.-d.-A., and A.F.J.-G.; Funding acquisition: L.F.M.; Investigation: A.F.J.-G., J.M.R.-d.-A. and L.F.M.; Resources: L.F.M.; Validation: J.M.R.-d.-A., A.F.J.-G., and L.F.M.; Writing—original draft: J.M.R.-d.-A. and L.F.M.; Writing—review and editing: J.M.R.-d.-A. and L.F.M.; Methodology: L.F.M., A.F.J.-G., and J.M.R.-d.-A.; Project administration: L.F.M. All authors have read and agreed to the published version of the manuscript.

Funding: Dirección General de Asuntos del Personal Académico de la Universidad Nacional Autónoma de México (DGAPA-UNAM), by grant number IN113220.

Acknowledgments: We thank (DGAPA-UNAM) for partial financial support by Grant IN113220. We also appreciate UNAM-Miztli-Super-Computing Center technical assistance by the project LANCADUNAM-DGTIC-030.

Conflicts of Interest: The authors declare no conflict of interest.

References

1. Edgar, J.H.; Hoffman, T.B.; Clubine, B.; Currie, M.; Du, X.Z.; Lin, J.Y.; Jiang, H.X. Characterization of Bulk Hexagonal Boron Nitride Single Crystals Grown by the Metal Flux Technique. *J. Cryst. Growth* **2014**, *403*, 110–113. [[CrossRef](#)]
2. Cao, X.K.; Clubine, B.; Edgar, J.H.; Lin, J.Y.; Jiang, H.X. Two-Dimensional Excitons in Three-Dimensional Hexagonal Boron Nitride. *Appl. Phys. Lett.* **2013**, *103*, 191106. [[CrossRef](#)]
3. Zhang, K.; Feng, Y.; Wang, F.; Yang, Z.; Wang, J. Two Dimensional Hexagonal Boron Nitride (2D-HBN): Synthesis, Properties and Applications. *J. Mater. Chem. C* **2017**, *5*, 11992–12022. [[CrossRef](#)]
4. Pease, R.S. Crystal Structure of Boron Nitride. *Nature* **1950**, *165*, 722–723. [[CrossRef](#)] [[PubMed](#)]
5. Pease, R.S. An X-Ray Study of Boron Nitride. *Acta Crystallogr.* **1952**, *5*, 356–361. [[CrossRef](#)]
6. Solozhenko, V.L.; Will, G.; Elf, F. Isothermal Compression of Hexagonal Graphite-like Boron Nitride up to 12 GPa. *Solid State Commun.* **1995**, *96*, 1–3. [[CrossRef](#)]
7. Kim, K.K.; Kim, S.M.; Lee, Y.H. A New Horizon for Hexagonal Boron Nitride Film. *J. Korean Phys. Soc.* **2014**, *64*, 1605–1616. [[CrossRef](#)]
8. Maestre, C.; Toury, B.; Steyer, P.; Garnier, V.; Journet, C. Hexagonal Boron Nitride: A Review on Selfstanding Crystals Synthesis towards 2D Nanosheets. *J. Phys. Mater.* **2021**, *4*, 044018. [[CrossRef](#)]
9. Watanabe, K.; Taniguchi, T.; Kanda, H. Direct-Bandgap Properties and Evidence for Ultraviolet Lasing of Hexagonal Boron Nitride Single Crystal. *Nat. Mater.* **2004**, *3*, 404–409. [[CrossRef](#)]
10. Said, A.; Debbichi, M.; Said, M. Theoretical Study of Electronic and Optical Properties of BN, GaN and B_xGa_{1-x}N in Zinc Blende and Wurtzite Structures. *Optik* **2016**, *127*, 9212–9221. [[CrossRef](#)]
11. Henriques, J.C.G.; Ventura, G.B.; Fernandes, C.D.M.; Peres, N.M.R. Optical Absorption of Single-Layer Hexagonal Boron Nitride in the Ultraviolet. *J. Phys. Condens. Matter* **2020**, *32*, 025304. [[CrossRef](#)] [[PubMed](#)]
12. Uosaki, K.; Elumalai, G.; Noguchi, H.; Masuda, T.; Lyalin, A.; Nakayama, A.; Taketsugu, T. Boron Nitride Nanosheet on Gold as an Electrocatalyst for Oxygen Reduction Reaction: Theoretical Suggestion and Experimental Proof. *J. Am. Chem. Soc.* **2014**, *136*, 6542–6545. [[CrossRef](#)] [[PubMed](#)]
13. Khan, M.H.; Jamali, S.S.; Lyalin, A.; Molino, P.J.; Jiang, L.; Liu, H.K.; Taketsugu, T.; Huang, Z. Atomically Thin Hexagonal Boron Nitride Nanofilm for Cu Protection: The Importance of Film Perfection. *Adv. Mater.* **2017**, *29*, 1603937. [[CrossRef](#)] [[PubMed](#)]
14. Guha, A.; Veetil Vineesh, T.; Sekar, A.; Narayanaru, S.; Sahoo, M.; Nayak, S.; Chakraborty, S.; Narayanan, T.N. Mechanistic Insight into Enhanced Hydrogen Evolution Reaction Activity of Ultrathin Hexagonal Boron Nitride-Modified Pt Electrodes. *ACS Catal.* **2018**, *8*, 6636–6644. [[CrossRef](#)]
15. Han, R.; Liu, F.; Wang, X.; Huang, M.; Li, W.; Yamauchi, Y.; Sun, X.; Huang, Z. Functionalised Hexagonal Boron Nitride for Energy Conversion and Storage. *J. Mater. Chem. A* **2020**, *8*, 14384–14399. [[CrossRef](#)]
16. Hasan Khan, M.S.; Mime, F.I.; Islam, M.R. Electronic and Optical Properties of Sn Doped Hexagonal BN Monolayer: A First-Principles Study. In Proceedings of the 2020 IEEE Region 10 Symposium (TENSYP), Dhaka, Bangladesh, 5–7 June 2020; pp. 230–233.
17. Ramirez-de-Arellano, J.M.; Jiménez, G.A.F.; Magaña, L.F. Catalytic Effect of Ti or Pt in a Hexagonal Boron Nitride Surface for Capturing CO₂. *Crystals* **2021**, *11*, 662. [[CrossRef](#)]
18. Emsley, J. *Nature's Building Blocks: An A–Z Guide to the Elements*; Reprinted with Corrections; Oxford University Press: Oxford, UK, 2003; ISBN 978-0-19-850340-8.
19. Deng, C.; He, R.; Shen, W.; Li, M. Theoretical Analysis of Oxygen Reduction Reaction Activity on Single Metal (Ni, Pd, Pt, Cu, Ag, Au) Atom Supported on Defective Two-Dimensional Boron Nitride Materials. *Phys. Chem. Chem. Phys.* **2019**, *21*, 18589–18594. [[CrossRef](#)]
20. Deng, C.; He, R.; Wen, D.; Shen, W.; Li, M. Theoretical Study on the Origin of Activity for the Oxygen Reduction Reaction of Metal-Doped Two-Dimensional Boron Nitride Materials. *Phys. Chem. Chem. Phys.* **2018**, *20*, 10240–10246. [[CrossRef](#)]

21. Giannozzi, P.; Andreussi, O.; Brumme, T.; Bunau, O.; Buongiorno Nardelli, M.; Calandra, M.; Car, R.; Cavazzoni, C.; Ceresoli, D.; Cococcioni, M.; et al. Advanced Capabilities for Materials Modelling with Quantum ESPRESSO. *J. Phys. Condens. Matter* **2017**, *29*, 465901. [[CrossRef](#)]
22. Hohenberg, P.; Kohn, W. Inhomogeneous Electron Gas. *Phys. Rev.* **1964**, *136*, B864–B871. [[CrossRef](#)]
23. Kohn, W.; Sham, L.J. Self-Consistent Equations Including Exchange and Correlation Effects. *Phys. Rev.* **1965**, *140*, A1133–A1138. [[CrossRef](#)]
24. Cottenier, S. *Density Functional Theory and the Family of (L)APW-Methods: A Step-by-Step Introduction*, 2nd ed.; Center for Molecular Modeling (CMM) & Department of Materials Science and Engineering (DMSE), Ghent University: Ghent, Belgium, 2013.
25. Troullier, N.; Martins, J. A Straightforward Method for Generating Soft Transferable Pseudopotentials. *Solid State Commun.* **1990**, *74*, 613–616. [[CrossRef](#)]
26. Perdew, J.P.; Burke, K.; Ernzerhof, M. Generalized Gradient Approximation Made Simple [Phys. Rev. Lett. 77, 3865 (1996)]. *Phys. Rev. Lett.* **1997**, *78*, 1396. [[CrossRef](#)]
27. Monkhorst, H.J.; Pack, J.D. Special Points for Brillouin-Zone Integrations. *Phys. Rev. B* **1976**, *13*, 5188–5192. [[CrossRef](#)]
28. Lindan, P.J.D.; Harrison, N.M.; Gillan, M.J.; White, J.A. First-Principles Spin-Polarized Calculations on the Reduced and Reconstructed TiO₂ (110) Surface. *Phys. Rev. B* **1997**, *55*, 15919–15927. [[CrossRef](#)]
29. Bohm, D.; Pines, D. A Collective Description of Electron Interactions: III. Coulomb Interactions in a Degenerate Electron Gas. *Phys. Rev.* **1953**, *92*, 609–625. [[CrossRef](#)]
30. Lucarini, V. (Ed.) *Kramers-Kronig Relations in Optical Materials Research*; Springer Series in Optical Sciences; Springer: New York, NY, USA, 2005; ISBN 978-3-540-23673-3.
31. Jiménez-González, A.F.; Ramírez-de-Arellano, J.M.; Magaña, L.F. Substantial Variations in the Optical Absorption and Reflectivity of Graphene When the Concentrations of Vacancies and Doping with Fluorine, Nitrogen, and Oxygen Change. *Int. J. Mol. Sci.* **2021**, *22*, 6832. [[CrossRef](#)]
32. Kokalj, A. XCrySDen—A New Program for Displaying Crystalline Structures and Electron Densities. *J. Mol. Graph. Model.* **1999**, *17*, 176–179. [[CrossRef](#)]